Microelectronic Engineering 86 (2009) 414–420

Contents lists available at ScienceDirect

Microelectronic Engineering

journal homepage: www.elsevier.com/locate/mee

TaN_x thin films as copper barriers sputter-deposited at various NH_3-to-Ar flow ratios

Jem Kun Chen [a,*], Chia-Hao Chan [b], Shiao-Wei Kuo [c], Feng-Chih Chang [b]

[a] Department of Polymer Engineering, National Taiwan University of Science and Technology, 43, Sec 4, Keelung Rd, Taipei 106, Taiwan, ROC
[b] Institute of Applied Chemistry, National Chiao-Tung University, Hsinchu 30043, Taiwan, ROC
[c] Department of Materials and Optoelectronic Science, Center for Nanoscience and Nanotechnology, National Sun Yat-Sen University, Kaohsiung, Taiwan

ARTICLE INFO

Article history:
Received 7 May 2008
Received in revised form 6 October 2008
Accepted 8 December 2008
Available online 16 December 2008

Keywords:
TaN_x thin film
Radio frequency sputtering
Diode

ABSTRACT

To optimize the performance of copper diffusion barriers, we deposited TaN_x thin films through radio frequency (RF) sputtering at various flow ratios of the reactive gases NH_3 and Ar. The composition of the film changed from Ta_2N to TaN, as evidenced from deposition rates and N-to-Ta ratios, when we increased the NH_3-to-Ar flow ratio from 0.075 to 0.3. Furthermore, the structure of the TaN_x thin film transformed from body-centered cubic (BCC) to face-centered cubic (FCC) to nanocrystalline upon increasing the NH_3-to-Ar flow rate, as revealed by the three steps in the rate of formation of the TaN_x films during the sputtering process. When incorporated in $Cu/TaN_x/n^+np^+$ diodes, the thermal stability of the TaN_x thin film—measured in terms of the leakage current remaining below 3 μA—increased from 450 to 550 °C upon increasing the NH_3-to-Ar flow ratio from 0.075 to 0.3. It appears that the NH_3-to-Ar flow ratio influences the properties of TaN_x films predominantly through modification of the crystal structure.

1. Introduction

Copper metal is the material of choice for ultralarge scale integration because of its lower bulk resistivity (1.62 μΩ cm), higher melting point (1084 °C), and improved electromigration resistance and stress-voiding resistance relative to those of aluminum and aluminum alloys (e.g., Al–Si and Al–Si–Cu) [1,2]. Copper has also emerged as an alternative interconnect material to replace Al and its alloys in deep submicrometer integrated circuits [3]. Because copper diffuses rapidly into SiO_2 or Si, and even reacts with Si at ca. 200 °C [4], effective diffusion barriers are needed between the Cu components and the SiO_2 and Si substrates of microelectronic devices. The solubility of Ta in Cu (and vice versa) is very low in the solid state [5] and silicide formation occurs only at relatively high temperatures [6]; thus, Ta-based layers are suitable diffusion barriers for Cu metallization [7,8]. Many diffusion barriers for copper metallization have been reported, including transition metal barriers (Ta, W), transition metal nitrides (TiN, TaN, WN) [9], and a transition metal boride (TiB_2) [10]. Amorphous ternary diffusion barriers, such as (Ti, Ta)SiN [11,12], are especially attractive because of their high thermal stability when in contact with copper layers.

Three structures have been observed for thin Ta films: thermodynamically stable body-centered cubic (BCC) α-Ta [13], metastable tetragonal β-Ta [14], and, more rarely, a face-centered cubic (FCC) phase [15]. Depending on the deposition parameters, a deposited Ta layer might consist of one or a mixture of these three phases [15]. The parameters determining the phase transformation are the annealing temperature and time [16,17], the annealing ambience, the substrate material, and the film thickness [18]. Ta adheres strongly to Cu [19], but only moderately to SiO_2 [20]. The feasibility of growing TaN thin films has been investigated extensively, particularly in terms of controlling the phase and microstructure of the TaN films to tightly control their barrier properties [21,22]. Investigations into the properties of single-layer TaN barriers have indicated that cubic TaN barriers normally exhibit the highest chemical inertness and thermal stability [23–25]. Because of the polycrystalline structure of Ta, grain boundary diffusion of Cu atoms becomes relevant at elevated temperatures [26]. One way to improve the thermal stability of Ta barrier layers is the addition of N atoms during the deposition process. Several reports describe how the phase composition and microstructure of as-deposited TaN films depend on the N content [27,28].

In this study we aimed to elucidate the properties of TaN_x barriers deposited onto SiO_2 and to compare them with those of TaN_x films deposited using mixtures of NH_3 and argon gases. We have used glancing angle X-ray diffraction (XRD) measurements and transmission electron microscopy (TEM) investigations to determine the structural and compositional changes in the layer stacks and X-ray photoelectron spectroscopy (XPS) to measure Cu silicide formation and to monitor changes in the concentrations of all atoms. Although there is a growing interest in graded Ta–TaN barrier layer stacks, little is known about their microstructures and thermal stabilities when incorporated in $Cu/TaN_x/n^+np^+$ diode systems. Thus, we fabricated $Cu/TaN_x/n^+np^+$ diodes and measured

* Corresponding author. Tel.: +886 2 27376516; fax: +886 2 27376544.
E-mail address: jkchen@mail.ntust.edu.tw (J.K. Chen).

0167-9317/$ - see front matter © 2008 Published by Elsevier B.V.
doi:10.1016/j.mee.2008.12.011

their leakage currents to determine the thermal stabilities of the TaN_x diffusion barriers after rapid thermal annealing (RTA) [29].

2. Experimental

For studies of graded Ta–TaN diffusion barriers, 4-in. thermally oxidized n-type silicon wafers having {1 1 1} planes of a thickness of 525 ± 25 μm were utilized as substrates. Thermal oxidation was performed at a temperature of 1000 °C for 120 min in an oxygen ambient to grow 140-nm-thick SiO_2 films. The wafers were cut into squares (1 × 1 cm) and then standard Radio Corporation of America (RCA) [30] cleaning was performed prior to loading the wafers into the load-lock. The TaN_x thin films were deposited through radio frequency (RF) reactive sputtering, using a mixture of NH_3 and Ar as the reactive gases under an RF power of 300 W. The base pressure in the physical vapor deposition (PVD) chamber was 3×10^{-5} Pa and the target-to-substrate distance was 150 mm.

To vary the nitrogen content in the sputter chamber, the NH_3-to-Ar flow ratios were chosen to be 0.075, 0.100, 0.125, 0.150, 0.175, 0.200, 0.225, and 0.300 under a sputtering pressure of 4.0 Pa. The thickness of each barrier was controlled precisely at 25 nm. All samples were then annealed under a pressure of 10^{-4} Pa at 650 °C for 3 h. Glancing angle XRD measurements [angle of incidence (ω) = 2°] were performed at room temperature in the parallel beam geometry with Cu Kα radiation (λ = 15.418 nm) and thin film equipment. The registered diffraction angle (2θ) ranged from 20° to 95° with a step size ($\Delta 2\theta$) of 0.05° and a measuring time of 40 s/step. To identify the phase of the deposited films and the crystal structure morphology, TEM investigations were performed using a JEOL 120EX microscope. The deposition rates and roughnesses of the TaN_x thin films were measured using cross-sectional TEM and atomic force microscope (AFM), respectively. XPS was used to analyze the N and Ta contents in the TaN films; the N-to-Ta ratio was estimated from these data.

The thermal failure of the TaN_x thin films in $Cu/TaN_x/n^+np^+$ diodes was tested in terms of the leakage current (Fig. 1). The thicknesses of n^+, n, and p^+ layers in the n^+np^+ diode (purchased from general semiconductor) were 20, 18, and 490 μm, respectively. Low-temperature oxide (LTO), glass, and medium-temperature oxide (MTO), having thicknesses of ca. 500, 800, and 700 nm, respectively, were utilized to isolate each diode. TaN_x barrier films having thicknesses of 25 nm were deposited onto the n^+np^+ surfaces at NH_3-to-Ar flow ratios of 0.075, 0.175, and 0.3 in the sputtering chamber. Next, copper films (thickness: 60 nm) were deposited on the TaN_x films through RF reactive sputtering with argon under a pressure of 3×10^{-5} Pa. The as-deposited $Cu/TaN_x/n^+np^+$ diodes were then subjected to RTA in a rapid thermal vacuum annealer for 10 min under an argon ambient at temperatures ranging from 450 to 650 °C (accuracy: ±1 °C). A forward voltage

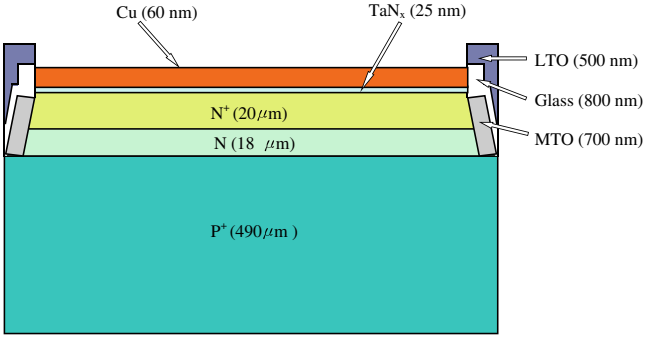

Fig. 1. Structure of Cu/TaN_x (25 nm)/n^+np^+ diodes used for measurement of the leakage current at various temperatures.

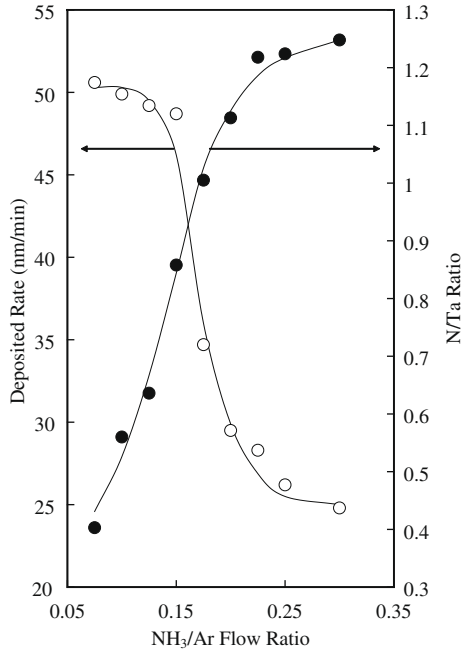

Fig. 2. Deposition rates and N-to-Ta ratios of TaN_x thin films plotted with respect to the NH_3-to-Ar flow ratio, after annealing at 600 °C for 10 min.

was applied to the $Cu/TaN_x/n^+np^+$ diode, with the negative terminal connected to the copper electrode and the positive terminal applied to the p^+ layer electrode. The *I–V* curves were recorded to monitor the current passing through the diode (from p^+ to the copper electrode), which placed on a hotplate to vary the temperature from room temperature to 650 °C as the forward voltage (−5 V)

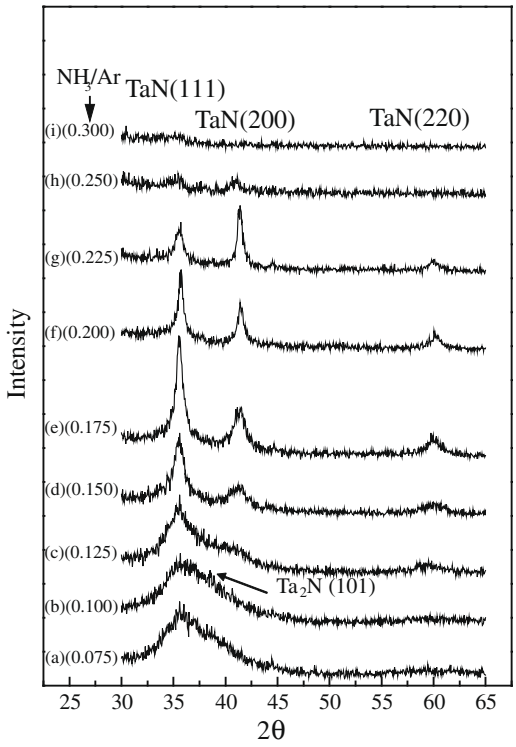

Fig. 3. XRD spectra of TaN_x thin films deposited at NH_3-to-Ar flow ratios of (a) 0.075, (b) 0.1, (c) 0.125, (d) 0.15, (e) 0.175, (f) 0.2, (g) 0.225, (h) 0.25, and (i) 0.3, after annealing at 600 °C for 10 min.

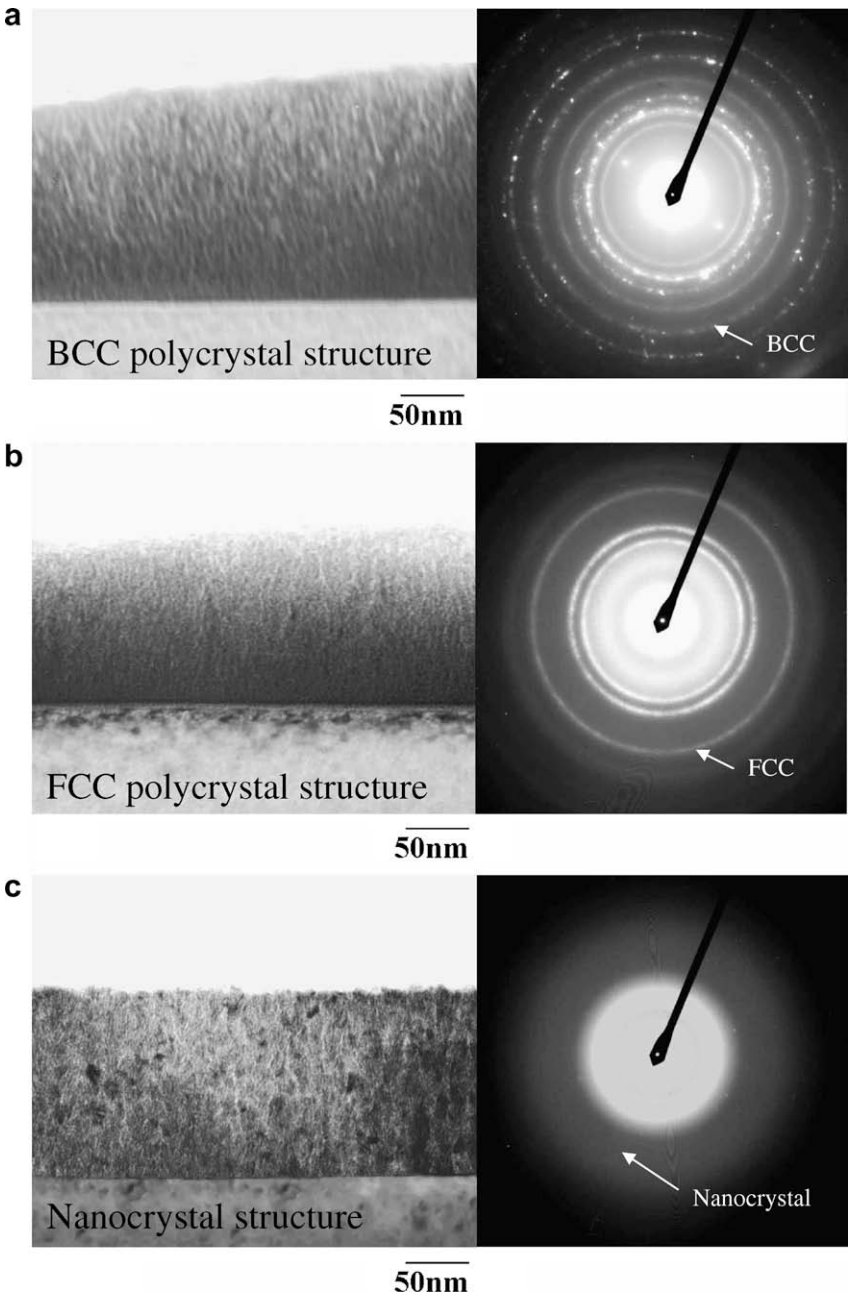

Fig. 4. Bright-field cross-sectional TEM images and diffraction patterns of TaN_x thin films deposited at NH_3-to-Ar flow ratios of (a) 0.075, (b) 0.175, and (c) 0.3, after annealing at 600 °C for 10 min.

was applied on the diode. To evaluate the thermal properties, the leakage currents of the $Cu/TaN_x/n^+np^+$ diodes were measured using a Sony Tektronix 370A instrument operated at an applied potential of −5 V under temperatures ranging from 450 to 650 °C.

3. Results and discussion

3.1. Deposition rate and composition of the TaN_x film

Fig. 2 displays the deposition rates of the TaN_x thin films and the N-to-Ta ratios as estimated from XPS data of the TaN_x films prepared at various NH_3-to-Ar flow ratios. The initial deposition rate of the TaN_x thin films was ca. 50 nm/min when the NH_3-to-Ar flow ratio ranged from 0.075 to 0.15, but it decreased rapidly [31] when the flow ratio increased from 0.175 to 0.25. In addition, the N-to-Ta ratio increased from 0.4 to 0.56 when the NH_3-to-Ar flow ratio increased from 0.075 to 0.1. The observation suggests that a composite of Ta and Ta_2N formed in the thin films when the N-to-Ta ratio was less than 0.5. We ascribe the increasing N-to-Ta ratio to the diffusion of elemental N—arising from the mixed NH_3 and Ar gases—into the vacancies around the Ta structure. The rapidly decreasing rate of deposition as the NH_3-to-Ar flow ratio increased from 0.15 to 0.2 suggested that the composition of the thin film transformed from Ta_2N to TaN, corresponding to an increase in the N-to-Ta ratio from 0.86 to 1.11. We believe that vacancies around the Ta atoms were occupied gradually by N atoms, which induced the transformation from Ta_2N to TaN and led to the decrease in the deposition rate. The TaN thin film formed gradually when the NH_3-to-Ar flow ratio was greater than 0.125. The deposi-

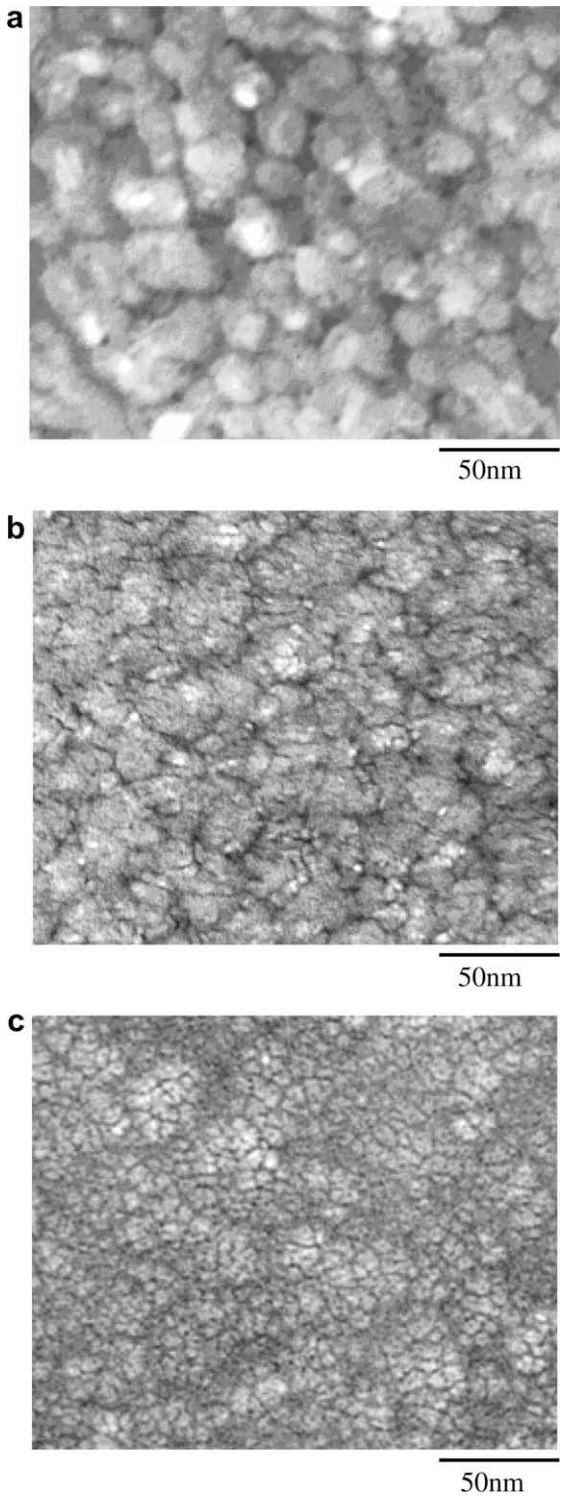

Fig. 5. Bright-field plan-view TEM images of TaN_x thin films deposited at NH_3-to-Ar flow ratios of (a) 0.075, (b) 0.175, and (c) 0.3, after annealing at 600 °C for 10 min.

tion rate decreased gradually, reaching 25 nm/min when flow ratio increased from 0.2 to 0.3, due to the formation of the TaN thin film. The N-to-Ta ratio was greater than one when the NH_3-to-Ar flow ratios ranged from 0.2 to 0.3 because the interstitial regions around the TaN structure became occupied by N atoms. In addition, the N-to-Ta ratio in the TaN_x films reached an approximate constant value of 1.28 when the NH_3-to-Ar flow ratio reached 0.3; in this case, the occupation of N atoms in the interstitial regions around the TaN structure approached saturation. These observations suggest that multi-phase mixed-composite Ta and Ta_2N films were formed at low NH_3-to-Ar flow ratios (0.075–0.1), whereas TaN films were formed at high flow ratios (0.125–0.2).

3.2. Structure and morphology of the TaN_x films

Fig. 3 displays the XRD spectra obtained from the TaN_x thin films deposited at the various NH_3-to-Ar flow ratios. The broad peak that appears at an angle of 38.7° when the NH_3-to-Ar flow ratio ranged from 0.075 to 0.1 corresponds to the (101) reflections of hexagonal Ta_2N. Thus, this broad peak reflects the presence of a composite of Ta and Ta_2N in BCC structures, where the N/Ta ratio ranged from 0.4 to 0.56. The N-to-Ta ratio increased continuously as the flow ratio increased from 0.075 to 0.1, revealing that the thin films were composed mainly of Ta and Ta_2N. When the NH_3-to-Ar flow ratio increased further (from 0.15 to 0.225), TaN predominated in the films, as evidenced by the lack of intense peaks for Ta_2N in the XRD spectra and the presence of sharp peaks at diffraction angles of 35.2°, 41.7°, and 60.9° corresponding to the (111), (200), and (220) reflections, respectively, of TaN having an FCC structure. Therefore, the polycrystalline structures transformed from BCC at flow ratios from 0.075 to 0.1 to FCC at flow ratios from 0.125 to 0.225. The peaks corresponding to the FCC structure were absent when the NH_3-to-Ar flow ratio ranged from 0.25 to 0.3, revealing that the TaN structure transformed from FCC to nanocrystalline [32]. We suspect that the interstitials around the TaN structure were occupied by N atoms that impeded the formation of the FCC structure in the TaN films when NH_3-to-Ar flow ratios increased from 0.225 to 0.3, thereby inducing the formation of nanocrystalline TaN films.

Fig. 4 displays bright-field cross-sectional TEM images and transmission electron diffraction patterns taken from the surfaces of TaN_x films prepared at various NH_3-to-Ar flow ratios. Series of diffused concentric rings and sharp concentric rings represent nanocrystal (amorphous) and polycrystalline structure, respectively. The several spotted rings having larger radii and halo rings having smaller radii (they contain only a few spots) correspond to the interplanar spacings and interatomic distances, respectively, in Fig. 4a and b, suggesting that the TaN_x films possessed BCC and FCC polycrystalline structures when the NH_3-to-Ar flow ratios were 0.075 and 0.175, respectively. The halo rings correspond to slightly longer interatomic distances and the spotted ones correspond to shorter ones, relative to those of the polycrystalline structures. The TaN_x film in Fig. 4c exhibits only halo rings in its transmission electron diffraction patterns because of its nanocrystalline structure. When the NH_3-to-Ar flow ratio was 0.075, the Ta_2N thin film that formed had the BCC polycrystalline structure, as verified by the ring pattern displayed in Fig. 4a and the bright-field cross-sectional TEM images demonstrating a columnar-like structure. After increasing the NH_3-to-Ar flow ratio to 0.175, the Ta_2N thin film transformed into a TaN thin film having an FCC polycrystalline domain, as verified in Fig. 4b and by the bright-field cross-sectional TEM image, which indicated a preferred (111) orientation, consistent with the XRD spectrum in Fig. 3e [33]. When the NH_3-to-Ar flow ratio increased to 0.300, the TaN thin film possessed a lattice-like nanocrystalline structure, as evidenced by the bright-field cross-sectional TEM image in Fig. 4c, which corresponded to the XRD dispersive peaks in Fig. 3i. Fig. 5 displays bright-field plan-view TEM images of the TaN_x thin films deposited at various NH_3-to-Ar flow ratios. The grain sizes decreased from 23.8 to 15.1 to 9.3 nm when the NH_3-to-Ar flow ratios increased from 0.075 to 0.175 to 0.300. In addition, Fig. 6 displays the morphology on the TaN_x film surface when the NH_3-to-Ar flow ratios increased from 0.075 to 0.175 to 0.300. Table 1 summarizes the grain sizes

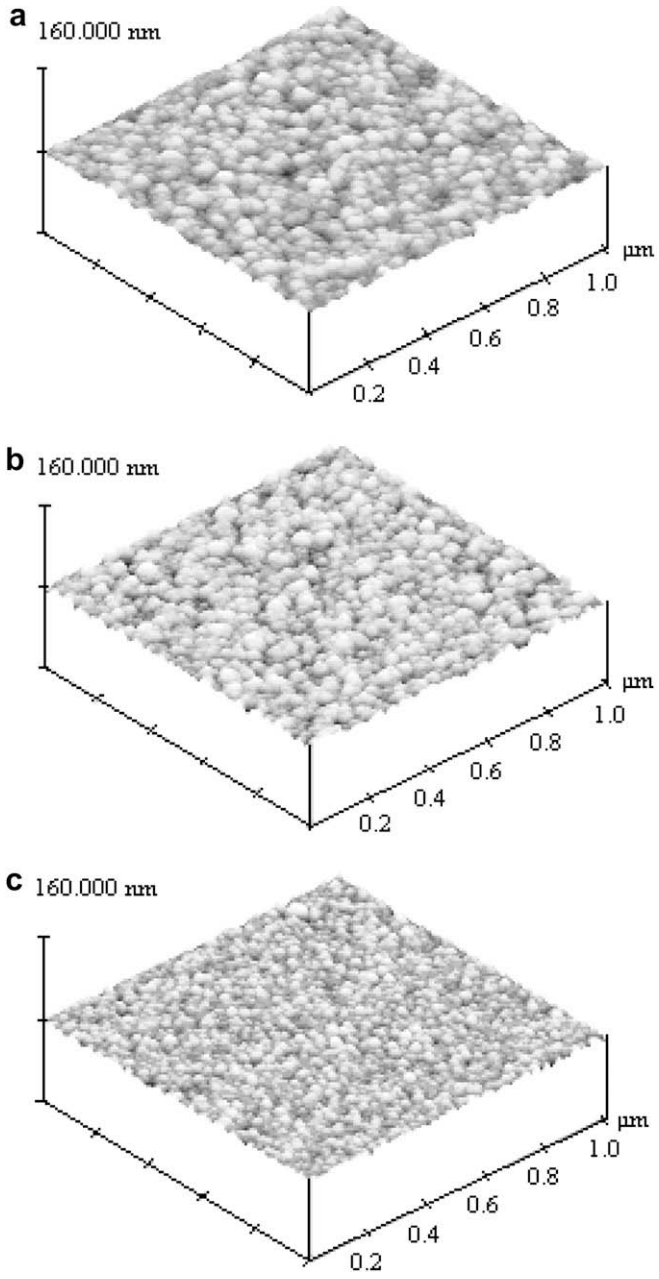

Fig. 6. AFM images of TaN_x thin films deposited at NH_3-to-Ar flow ratios of (a) 0.075, (b) 0.175, and (c) 0.3, after annealing at 600 °C for 10 min.

and surface roughnesses estimated from AFM images as shown in Fig. 6.

Fig. 7 displays the grain densities calculated from the TEM images and the resistivities of the TaN_x thin films plotted with respect to NH_3-to-Ar flow ratio. The grain density was approximately 2.3 when the NH_3-to-Ar flow ratio was less than 0.15, consistent with Ta_2N films having BCC polycrystalline domains and grain sizes of 23.8 nm. When the NH_3-to-Ar flow ratio was greater than 0.175, the grain density increased rapidly because of the formation of FCC polycrystalline and nanocystalline domains. We define the midpoint of the flow ratios from 0.175 to 0.225 as the critical ratio representing the transition from the BCC to FCC polycrystalline domains. The resistivity increased only gradually upon increasing of NH_3-to-Ar flow ratio from 0.075 to 0.15, but then it increased rapidly when the NH_3-to-Ar flow ratio was greater than the critical ratio as a result of the formation of FCC polycrystalline TaN films.

Table 1
Grain sizes and roughnesses, estimated from AFM images, for TaN_x films prepared at various flow ratios.

Reactive gas flow ratio (NH_3/Ar)	Grain size (nm)	Surface roughness (nm)
0.075	23.8	5.3
0.175	15.1	3.7
0.300	9.3	1.8

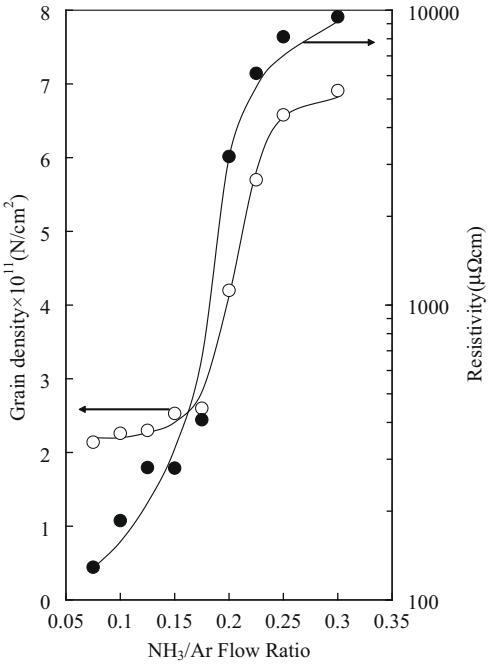

Fig. 7. Grain densities and resistivities of TaN_x thin films deposited at various NH_3-to-Ar flow ratios, after annealing at 600 °C for 10 min.

Thus, the resistivities of the TaN_x thin films were related to their structures and grain densities. Increasing the N content around the Ta atoms varied the structure and composition of the TaN_x film, thereby increasing the grain density. Therefore, the resistivity of the TaN_x films increased upon increasing the N atom content and, thereby, the crystal structure. The resistivity of the TaN_x films, in terms of their crystal structures, exhibited the following trend: BCC-Ta_2N < FCC-TaN < nanocrystal-TaN.

3.3. Leakage current as a measure of thermal stability

To analyze the thermal stability, we measured the leakage current under a forward voltage of −5 V for Cu/$TaN_{0.99}$ (25 nm)/n^+np^+ diodes at room temperature and at 500, 550, and 600 °C (Fig. 8). At room temperature, the electrons were obstructed by the TaN_x film, causing the leakage current of the diode to be 0.5 μA under the applied forward voltage. When we increased the temperature to 500 °C, the leakage current increased slightly to 2.5 μA at −5 V, suggesting that some of the copper atoms had diffused through the barrier in the Cu/$TaN_{0.99}$ (25 nm)/n^+np^+ diode. The leakage current increased to 15 μA at −5 V due to the diffusion of Cu through the TaN_x barrier layer into the n^+np^+ diode as temperature closed to 550 °C. When the temperature approached 600 °C, the leakage current increased to 1220 μA, reflecting the collapse of the TaN_x barrier layer. We consider a TaN_x diffusion barrier to be thermally stable if the leakage current remains less than 3 μA [23]. Table 2

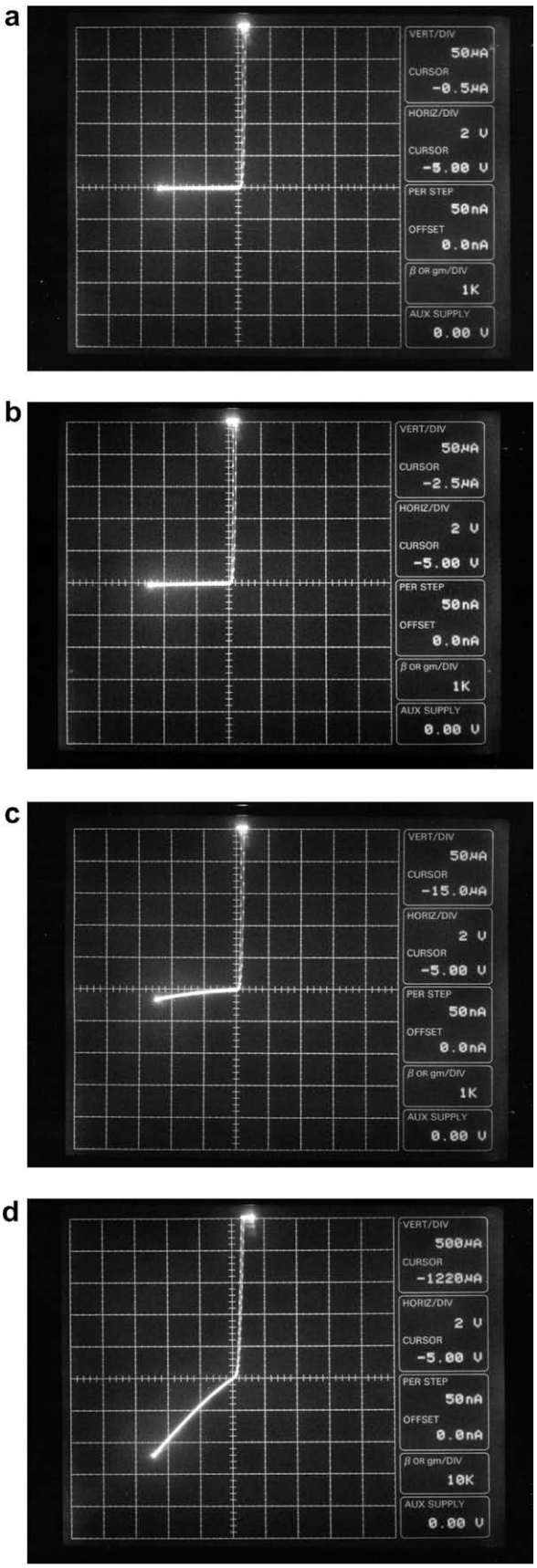

Fig. 8. *I–V* curves obtained after a forward voltage of −5 V was applied to Cu/$TaN_{0.99}$ (25 nm)/n^+np^+ diode to measure the current at (a) room temperature and (b) 500, 550, and 600 °C.

Table 2
Highest thermal stability temperatures of Cu/TaN_x/n^+np^+ samples.

Reactive gas flow ratio (NH_3/Ar)	Cu/TaN_x (25 nm)/n^+np^+	Highest thermal stability temperature[a] (°C)
0.075	Cu/$TaN_{0.42}$ (25 nm)/n^+np^+	450
0.175	Cu/$TaN_{0.99}$ (25 nm)/n^+np^+	500
0.300	Cu/$TaN_{1.28}$ (25 nm)/n^+np^+	550

[a] Defined as the highest temperature at which the leakage current was less than 3 μA.

summarizes the highest thermal stability temperatures of the Cu/TaN_x/n^+np^+ diodes (x = 0.42, 0.99, and 1.28) prepared at NH_3-to-Ar flow ratios of 0.075, 0.175, and 0.300. The highest thermal stability temperatures for the TaN_x diffusion barriers increased upon increasing the N-to-Ta ratio because of the increasing electron charge cloud density arising from the presence of N atoms, which resisted the diffusion of Cu through the TaN_x film through repulsive forces [31]. Thus, the optimal thermal stability occurred for TaN_x films having a value of x close to 1.28.

4. Conclusions

TaN_x thin films deposited at increasing NH_3-to-Ar flow ratios underwent a structural transition from BCC to FCC to nanocrystalline, as evidenced by their deposition rates, N-to-Ta ratios, and grain densities. The mixed NH_3-to-Ar gases induced the formation of TaN_x films having various structures and compositions. Furthermore, the TaN_x films were composed mainly of Ta_2N and TaN in their various structures upon increasing the NH_3-to-Ar flow ratio from 0.075 to 0.3, as deduced from the three steps in the plot of the deposition rate. The thermal stabilities of the TaN_x films depended predominantly on their crystal structures and compositions. Increasing the N-to-Ta ratio enhanced the thermal stability of the corresponding Cu/TaN_x/n^+np^+ diode structure, thereby approaching the optimal thermal properties for a Cu barrier.

Acknowledgment

We thank the National Science Council of the Republic of China for supporting this research financially.

References

[1] J. Li, T.E. Seidel, J.W. Mayer, MRS Bull. 19 (1994) 15.
[2] K.S. Gadre, T.L. Alford, J.W. Mayer, Appl. Phys. Lett. 79 (2001) 3260.
[3] S.P. Murarka, Mater. Sci. Eng. R19 (1997) 87.
[4] L. Stolt, A. Chrai, F.M. D'Heurle, O.M. Fryer, J.M.E. Harper, J. Vac. Sci. Technol. A 9 (1991) 1501.
[5] P.R. Subramanian, D.E. Laughlin, Bull. Alloy Phase Diagrams 10 (1989) 652.
[6] L. Liu, Y. Wang, H. Gong, J. Appl. Phys. 90 (2001) 416.
[7] L.A. Clevenger, N.A. Bojarczuk, K. Holloway, J.M.E. Harper, C. Cabral, R.G. Schad, F. Cardone, L. Stolt, J. Appl. Phys. 73 (1993) 300.
[8] T. Laurila, K. Zeng, J.K. Kivilahti, J. Molarius, I. Suni, J. Appl. Phys. 88 (2000) 3377.
[9] S.Q. Wang, MRS Bull. 19 (1994) 30.
[10] J. Pelleg, G. Sade, J. Appl. Phys. 91 (2002) 6099.
[11] J.-T. No, J.-H. O, C. Lee, Mater. Chem. Phys. 63 (2000) 44.
[12] D. Fisher, T. Scherg, J.G. Bauer, H.-J. Schultz, C. Wenzel, Microelectron. Eng. 50 (2000) 459.
[13] M.H. Mueller, Scr. Metall. 11 (1977) 693.
[14] A. Arakcheeva, G. Chapuis, V. Grinevitch, Acta Cryst. B 58 (2002) 1.
[15] P.N. Baker, Thin Solid Films 14 (1972) 3.
[16] L.A. Clevenger, A. Mutscheller, J.M.E. Harper, C. Cabral Jr., K. Barmak, J. Appl. Phys. 72 (1992) 4918.
[17] M.H. Read, C. Altman, Appl. Phys. Lett. 7 (1965) 51.

[18] R. Hoogeveen, M. Moske, H. Geisler, K. Samwer, Thin Solid Films 275 (1996) 203.
[19] L. Chen, B. Ekstrom, J. Kelber, Mater. Res. Soc. Symp. Proc. 564 (1999) 287.
[20] M. Lane, R.H. Dauskardt, N. Krishna, I. Hashim, J. Mater. Res. 15 (2000) 203.
[21] J.C. Lin, G. Chen, C. Lee, J. Electrochem. Soc. 146 (1999) 1835.
[22] Y.J. Lee, B.S. Suh, M.S. Kwon, C.O. Park, J. Appl. Phys. 85 (1999) 1927.
[23] K. Wakasugi, M. Tokunaga, T. Sumita, H. Kubota, M. Nagata, Y. Honda, Physica B 239 (1997) 29.
[24] Y.J. Zhang, P.X. Yan, Z.G. Wu, W.W. Zhang, G.A. Zhang, W.M. Liu, Q.J. Xue, Adv. Mater. 202 (2005) 95.
[25] M.H. Tsai, S.C. Sun, C.E. Tsai, S.H. Chuang, H.T. Chiu, J. Appl. Phys. 79 (1996) 6932.
[26] D. Fischer, O. Meissner, B. Bendjus, J. Schreiber, M. Starvev, C. Wenzel, Surf. Interface Anal. 25 (1997) 522.
[27] M. Stavrev, D. Fischer, C. Wenzel, K. Drescher, N. Mattern, Thin Solid Films 307 (1997) 79.
[28] C.-S. Shin, Y.-W. Kim, D. Gall, J.E. Greene, I. Petrov, Thin Solid Films 402 (2002) 172.
[29] M.T. Wang, Y.C. Lin, M.C. Chen, J. Electrochem. Soc. 135 (1998) 2538.
[30] E. Kolawa, J.S. Chen, J.S. Raid, P.J. Pokela, M.A. Nicolet, J. Appl. Phys. 70 (1991) 1369.
[31] T. Okamoto, M. Shimizu, A. Ohsaki, Y. Mashiko, K. Tsukamoto, T. Mastsukawa, S. Nagao, J. Appl. Phys. 62 (1987) 4465.
[32] X. Sun, E. Kolawa, J.S. Chen, J.S. Reid, M.-A. Nicolet, Thin Solid Films 236 (1993) 347.
[33] M. Takeyama, A. Noya, T. Sase, A. Ohta, J. Vac. Sci. Technol. B 14 (1996) 674.